Tracking the sarcoplasmic reticulum membrane voltage in muscle with a FRET biosensor

Colline Sanchez[1], Christine Berthier[1], Bruno Allard[1], Jimmy Perrot[1], Clément Bouvard[1], Hidekazu Tsutsui[2,3], Yasushi Okamura[2], and Vincent Jacquemond[1]

Ion channel activity in the plasma membrane of living cells generates voltage changes that are critical for numerous biological functions. The membrane of the endoplasmic/sarcoplasmic reticulum (ER/SR) is also endowed with ion channels, but whether changes in its voltage occur during cellular activity has remained ambiguous. This issue is critical for cell functions that depend on a Ca^{2+} flux across the reticulum membrane. This is the case for contraction of striated muscle, which is triggered by opening of ryanodine receptor Ca^{2+} release channels in the SR membrane in response to depolarization of the transverse invaginations of the plasma membrane (the t-tubules). Here, we use targeted expression of voltage-sensitive fluorescence resonance energy transfer (FRET) probes of the Mermaid family in differentiated muscle fibers to determine whether changes in SR membrane voltage occur during depolarization–contraction coupling. In the absence of an SR targeting sequence, FRET signals from probes present in the t-tubule membrane allow calibration of the voltage sensitivity and amplitude of the response to voltage-clamp pulses. Successful SR targeting of the probes was achieved using an N-terminal domain of triadin, which completely eliminates voltage-clamp–activated FRET signals from the t-tubule membrane of transfected fibers. In fibers expressing SR-targeted Mermaid probes, activation of SR Ca^{2+} release in the presence of intracellular ethyleneglycol-bis(β-amino-ethyl ether)-N,N,N',N'-tetra acetic acid (EGTA) results in an accompanying FRET signal. We find that this signal results from pH sensitivity of the probe, which detects cytosolic acidification because of the release of protons upon Ca^{2+} binding to EGTA. When EGTA is substituted with either 1,2-bis(o-aminophenoxy)ethane-N,N,N',N'-tetraacetic acid or the contraction blocker N-benzyl-p-toluene sulfonamide, we find no indication of a substantial change in the FRET response caused by a voltage change. These results suggest that the ryanodine receptor–mediated SR Ca^{2+} efflux is well balanced by concomitant counterion currents across the SR membrane.

Introduction

Ion fluxes across the cell plasma membrane generate electrical activity that plays a key role in the function of excitable and non-excitable tissues (Hodgkin and Huxley, 1952; Bertrán et al., 1995; Armstrong and Hille, 1998). Ion channels, pumps, and transporters are also present in the membrane of the ER/SR, where they either play a clearly identified role (Berridge, 1993; Meissner, 1994; Martonosi, 1996) or are presumed to do so (Kourie et al., 1996; Picollo and Pusch, 2005; Yazawa et al., 2007; Kuum et al., 2012). One of the most classic examples is the role of Ca^{2+} release channels and SR/ER Ca^{2+}-ATPase in Ca^{2+} cycling across the reticulum membrane to control contraction of smooth and striated muscles. In skeletal muscle, contraction is initiated when action potentials activate the voltage-sensing $Ca_V1.1$ proteins in the t-tubules, within a specific membrane region called the triad, where the membrane of one t-tubule is in close apposition with

the membrane of two terminal cisternae of SR. In turn, activated $Ca_V1.1$s open up type 1 ryanodine receptor (RYR1) Ca^{2+} release channels in the junctional SR membrane, through a protein–protein interaction coupling process (Schneider, 1994; Samsó, 2015). The resulting SR Ca^{2+} efflux increases cytosolic $[Ca^{2+}]$, which triggers contraction. So far, it is believed that during Ca^{2+} release, the voltage across the SR membrane is maintained near a resting value close to 0 mV because of a countercurrent of other ions (Somlyo et al., 1981; Smith et al., 1988; Oetliker, 1989; Fink and Veigel, 1996; Gillespie and Fill, 2008). However, the ER/SR membrane is not accessible to standard electrophysiology in intact cells, which has so far prevented determining whether changes in its electrical potential occur during cellular activity. In skeletal muscle, this question was experimentally challenged in the 1980s (Vergara et al., 1978; Baylor et al., 1984). However, results

[1]Université Claude Bernard Lyon 1, Institut NeuroMyoGène, Villeurbanne, France;   [2]Laboratory of Integrative Physiology, Graduate School of Medicine, Osaka University, Osaka, Japan;   [3]Bioscience and Bioengineering, Japan Advanced Institute of Science and Technology, Nomi, Ishikawa, Japan.

Correspondence to Vincent Jacquemond: vincent.jacquemond@univ-lyon1.fr.

were inconclusive, and because the approaches used at the time lacked target specificity, it could not be established whether the detected signals corresponded to a SR voltage change or resulted from other steps of excitation–contraction (EC) coupling. Here, we circumvented this problem by targeting voltage-sensing fluorescence resonance energy transfer (FRET) biosensors of the Mermaid family (Tsutsui et al., 2008) to the SR membrane of muscle fibers. Results suggest that the SR membrane voltage changes negligibly during muscle fiber activation, if at all.

Materials and methods

All experiments and procedures were performed according to the ethics principles of the French Department of Veterinary Services and the French Ministry for Higher Education and Research, in accordance with the guidelines of the local animal ethics committee of the University Claude Bernard Lyon 1, the French Ministry of Agriculture (decree 87/848), and the revised European Directive 2010/63/EU. All experiments were performed at room temperature (20–22°C).

Plasmid constructs

Biosensor cDNAs were derived from the original Mermaid cDNA (Tsutsui et al., 2008) and were all inserted into the modified pCS2+ vector for mammalian expression. Rv-Mermaid cDNA was designed by inserting Mermaid voltage-sensing domain (VSD) coding sequence in 3′ of mUKG and mKOκ coding sequences. Rv-Mermaid$^{D129E/Y235R}$ was designed by inserting mutations into codons 129 and 235 of the VSD S4-segment sequence to shift its voltage dependence toward more positive values (Tsutsui et al., 2013a,b). The VSD$^{D129E/Y235R}$ sequence was PCR amplified from pCS2+-Mermaid$^{D129E/Y235R}$ and was used to replace WT VSD sequence by in-frame insertion using EcoRI and XbaI sites. To trigger retention of the biosensor at the triadic SR, we fused in frame the cDNA sequence of human skeletal triadin (gift of V. Sorrentino, University of Siena, Siena, Italy) corresponding to residues 1–306 (T306). These residues are indeed necessary and sufficient for proper triadic localization (Rossi et al., 2014). T306 cDNA was amplified by PCR to generate appropriate XbaI and SacII restriction sites and was subcloned in-frame at the 3′ end of Rv-Mermaid$^{D129E/Y235R}$ into pCS2+. Another sequence of reticular biosensor was designed by replacing the 103-residue-long cytosolic N-terminal chain of Mermaid2 (Tsutsui et al., 2013b) by a 201-residue-long N-terminal chain comprising two di-arginine motifs (residues 29–35). Di-arginine motif located in the N-terminal cytosolic tail has been shown to be responsible for ER retention of phospholamban through a putative COP I–mediated transport (Sharma et al., 2010). After PCR amplification, the cDNA fragment corresponding to this so-called ER-N-terminal sequence was inserted in-frame and in place of the original 5′ end of Mermaid2 sequence using appropriate restriction enzymes.

In vivo transfection

The experimental protocol for in vivo transfection was approved by the Lyon University Animal Experimentation Committee. Expression was achieved by plasmid injection followed by electroporation according to previously described procedures

(Lefebvre et al., 2011). In brief, Swiss OF1 male mice 8–16 wk old were used. Transfection was performed so as to target both the flexor digitorum brevis (fdb) and interosseus muscles of the animals. Mice were anesthetized by isoflurane inhalation using a commercial delivery system (Univentor 400 Anesthesia Unit; Uninventor). Then, 20 µl of a solution containing 2 mg/ml hyaluronidase dissolved in sterile saline was injected into the footpads of each hind paw. 1 h later, the mouse was reanesthetized by isoflurane inhalation. A total volume of 20 µl of a solution containing 30–50 µg plasmid DNA diluted in NaCl 0.9% was injected into the footpads of the animal. After the injection, two gold-plated stainless steel acupuncture needles connected to the electroporation apparatus were inserted under the skin, near the proximal and distal portion of the foot, respectively. The standard protocol that we used consisted of 20 pulses of 130 V/cm amplitude and 20-ms duration delivered at a frequency of 2 Hz by a BTX ECM 830 square wave pulse generator (Harvard Apparatus). Muscle fiber isolation and experimental observations and measurements were performed 7–14 d later.

Preparation of muscle fibers and electrophysiology

Single fibers were isolated from the fdb and interosseus muscles using a previously described procedure (Jacquemond, 1997). Mice were anesthetized by isoflurane inhalation and killed by cervical dislocation before removal of the muscles. Muscles were treated with collagenase (type I; Sigma) for 60 min at 37°C in the presence of Tyrode's solution (see Solutions). Single fibers were then obtained by gentle trituration of the muscles within a 50-mm-wide culture µ-dish (Ibidi) filled with culture medium containing 10% FBS (MI199; Eurobio), the bottom of which had been first covered with a thin layer of silicone grease. Single fibers were then partially insulated with silicone grease so that only a 50–100-µm-long portion of the fiber extremity was left out of the silicone, as described previously (Jacquemond, 1997). In case of local expression of the constructs (Fig. 4), care was taken so that the expressing fiber region was outside of the silicone. Voltage clamp was performed with a micropipette filled with an intracellular-like solution (see Solutions). The tip of the micropipette was inserted through the silicone within the insulated part of the fiber and was crushed against the bottom of the chamber to reduce series resistance and ease intracellular equilibration of the micropipette solution. The micropipette was connected to an RK-400 patch-clamp amplifier (Bio-Logic) used in whole-cell voltage-clamp configuration. Command voltage pulse generation was achieved with an analogue-to-digital converter (Digidata 1440A; Axon Instruments) controlled by pClamp 9 software (Axon Instruments). Fibers were bathed in the TEA-containing extracellular solution (see Solutions). Analogue compensation was adjusted to further decrease the effective series resistance. Voltage-clamp steps were applied from a holding command potential of either –80 or 0 mV. For intracellular Ca^{2+} measurements shown in Fig. S4, the micropipette was filled with the intracellular-like solution also containing 0.2 mM of the Ca^{2+}-sensitive fluorescent indicator fluo-4 FF. In most experiments, muscle fiber contraction was prevented by the presence of a large concentration of EGTA in the intracellular-like solution (see Solutions). Alternatively, contraction

was prevented by using either 1,2-bis(*o*-aminophenoxy)ethane-*N,N,N′,N′*-tetraacetic acid (BAPTA) in the intracellular-like solution or *N*-benzyl-*p*-toluene sulphonamide (BTS) in the extracellular solution, as specified in the text.

Fluorescence measurements in voltage-clamped muscle fibers

All experiments were conducted with a Zeiss LSM 5 Exciter confocal microscope equipped with a 63× oil-immersion objective (numerical aperture, 1.4). For *x,y* confocal imaging of fibers expressing the Mermaid constructs, either excitation was provided by the 488-nm line of an argon laser and a 505-nm long-pass filter was used on the detection channel, or excitation was at 543 nm from a HeNe laser and fluorescence was collected at >560 nm. Both configurations provided essentially identical images. For detection of FRET changes in response to voltage-clamp pulses, the line-scan mode (*x,t*) of the microscope was used with the 458-nm line of the argon laser for excitation and simultaneous detection at 500 ± 25 nm (F_{500}, green traces) and >560 nm ($F_{>560}$, red traces). The line was always oriented along the main axis of the fibers. To improve detection and limit photobleaching, records were taken with the pinhole fully open (1-mm diameter). Even under these conditions, the signal-to-noise ratio of the voltage-induced FRET changes was in most cases rather poor, so that, in a given fiber for each tested pulse protocol, routinely three to five records (each at a different line position) were taken and averaged. FRET signals were expressed as the ratio $R = F_{>560}/F_{500}$ and normalized to the ratio R_0 at either –80 or 0 mV, as specified in the text. Fluorescence records at 500 and >560 nm were corrupted to some extent by time-dependent changes including photobleaching, the relative rate of which differed on the two channels. In addition, with all Mermaid and Rv-Mermaid constructs, there was a transient rise in fluorescence at the beginning of the records that was most obvious on the red channel (Fig. 1, B and E). These changes were observed in the absence of voltage-clamp pulses and were not systematically cancelled in the $F_{>560}/F_{500}$ ratio. To correct for them, we used two strategies that gave essentially the same results. The first method consisted of using bracketing records from the same fiber region, taken with no voltage-clamp pulses applied. Corresponding ratios were fitted with either a single exponential plus linear function or with the sum of two exponentials, and the fits were then used to normalize the test records. Alternatively, fits were achieved directly on the test records, using only the portions of traces where no voltage-induced response was present; the result was then extrapolated to the full record duration and used for normalization. Examples of such fits performed directly on the fluorescence traces are shown as insets in Fig. 1 (B and E) and Fig. 2 B.

For detection of fluo-4 FF fluorescence, excitation was at 488 nm, whereas detection was >505 nm. Image processing and analysis was performed using ImageJ (National Institutes of Health) and Microcal Origin (Microcal Software).

Fluorescence measurements in nigericin-treated muscle fibers

To test the effect of changes in pH on the FRET signal from SR-targeted Mermaid probes, transfected muscle fibers were treated with nigericin. For this, single isolated muscle fibers expressing the construct of interest were partially embedded into silicone grease so that they remained well maintained on the bottom of the chamber during the experiment. A thin polyethylene capillary perfusion system operating by gravity was used to change the composition of the extracellular solution in the immediate vicinity of the tested fiber. Fluorescence detection was performed using the *x,y* scanning mode of the microscope with the standard FRET configuration (458-nm excitation and simultaneous detection at 500 and >560 nm). Fibers were bathed in a solution containing (in mM) 140 potassium glutamate, 2 $MgCl_2$, 5 glucose, 5 Na_2-ATP, 5 HEPES, and 0.01 nigericin adjusted to pH 7.0 or 7.2, and the gravity perfusion system was used to test the effect of solutions of identical composition adjusted to a different pH value.

Cell culture and immunolabeling

COS-7 and HeLa cells were grown in 4.5 g/l glucose-containing Dulbecco's Modified Eagle Media (Eurobio) supplemented with 10%–15% FCS, 100 mM sodium pyruvate, 100 U/ml penicillin, and 100 µg/ml streptomycin at 37°C in a 5% CO_2 environment. Cells were seeded on glass coverslips 1 d before transfection and transfected with corresponding plasmids using FuGENE HD (Promega) or Polyfect (Qiagen). Immunolabeling was performed 48–72 h after transfection. Cells were first fixed with 2% paraformaldehyde diluted in PBS supplemented with 300 mM $MgCl_2$ and 30 mM $CaCl_2$ (PBS-CaMg) and permeabilized with 0.1% Triton X-100/50 mM glycine in PBS-CaMg. Nonspecific sites were blocked with 1% BSA in PBS-CaMg. Cells were then incubated overnight at 4°C with the following primary monoclonal antibodies diluted in 1% BSA in PBS-CaMg: monoclonal anti-GM130 (clone 35; 1:1,000; BD Transduction), anti-KDEL (10C3; 1:250; Abcam), or polyclonal anti-GRP78 BIP antibody (1:200; Abcam). A second blocking step was performed using normal goat serum 1% in PBS-CaMg. Cells were then incubated with either Hilyte Fluor647–conjugated anti-mouse secondary antibody (Anaspec) or Alexa Fluor 594–conjugated anti–rabbit IgG (Molecular Probes) diluted in 1% normal goat serum in PBS-CaMg (1:500 or 1:1,000, respectively) for 1 h at ambient temperature.

Incubations all took place in a humidified chamber, and cells were extensively washed in PBS-CaMg after each incubation. Immunolabeled samples were mounted in antifading medium (Vectashield; Vector Laboratories; or Dako mounting medium) and examined using a Zeiss LSM 5 Exciter confocal microscope equipped with a 63× oil-immersion objective.

Solutions

The extracellular solution used for voltage clamp contained (in mM) 140 TEA-methanesulfonate, 2.5 $CaCl_2$, 2 $MgCl_2$, 1 4-aminopyridine, 10 HEPES, and 0.002 tetrodotoxin. The standard intracellular-like solution contained (in mM) 130 potassium glutamate, 5 Na_2-ATP, 5 Na_2-phosphocreatine, 20 mM EGTA, 8 mM $CaCl_2$, 5.5 $MgCl_2$, 5 glucose, and 5 HEPES. In some experiments, BAPTA was used in place of EGTA at the same concentration (specified in text). Current-clamp experiments were performed in the presence of extracellular Tyrode's solution containing (in mM) 140 NaCl, 5 KCl, 2.5 $CaCl_2$, 2 $MgCl_2$, and 10 HEPES. In some experiments, the extracellular solution contained 50 µM BTS to block contraction. For all experiments with BTS, the intracellular
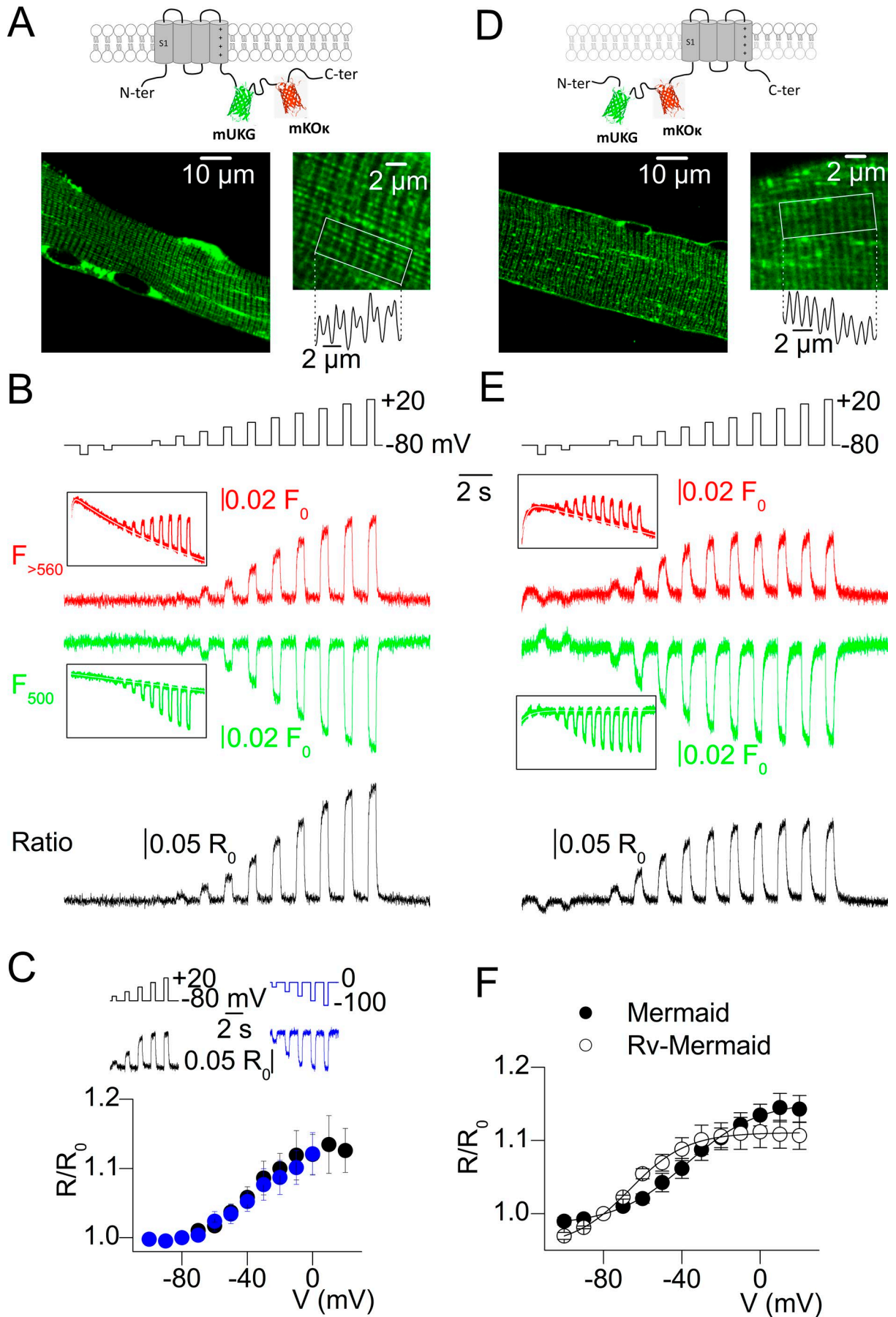
solution contained neither EGTA nor BAPTA. All solutions were adjusted to pH 7.20.

Statistics

Least-squares fits were performed using a Marquardt–Levenberg algorithm routine included in Microcal Origin (Originlab). Data values are presented as means ± SEM for n fibers.

Online supplemental material

Fig. S1 shows the sequence structure of plasma membrane– and SR membrane–targeted Mermaid-derived voltage sensors used in this project. Fig. S2 and Fig. S3 show the subcellular localization of Rv-Mermaid$^{D129E/Y235R}$ and of T306-Rv-Mermaid$^{D129E/Y235R}$ in COS-7 cells, respectively. Fig. S4 illustrates the disappearance and recovery of the FRET signal from T306-Rv-Mermaid$^{D129E/Y235R}$ upon voltage-dependent inactivation and recovery from inactivation of SR Ca^{2+} release, respectively. Fig. S5 shows the response of ER-Mermaid2^{-D129E} to t-tubule membrane depolarization. Fig. S6 shows the ER localization of ER-Mermaid2 in COS-7 and HeLa cells.

Results

FRET response of Mermaid biosensor to t-tubule membrane voltage changes

To measure changes in membrane voltage, we used fluorescent sensors of the Mermaid family composed of a VSD associated with the two fluorophores mUKG and mKOκ as FRET donor and acceptor, respectively (Tsutsui et al., 2008; Fig. S1). Expression of Mermaid in mouse muscle fibers yielded a transverse-banded fluorescence pattern under the form of successive double peaks separated by 2 μm (Fig. 1 A), consistent with the protein being present in the triadic region of the fibers. In response to voltage-clamp depolarizing steps from –80 mV, the detected changes in fluorescence (at 500 nm and >560 nm, upon 458-nm excitation) were consistent with voltage-dependent energy transfer between the two fluorophores mUKG and mKOκ (Fig. 1 B), providing evidence for localization of Mermaid in the t-tubule membrane of the muscle fibers. Main traces in Fig. 1 B have been corrected from time-dependent changes in fluorescence also observed when no voltage pulse was given. Similar changes

were previously reported for the fluorescent proteins mOrange2 (Shaner et al., 2008) and mNeptune (Chu et al., 2014) and interpreted as resulting from photoactivation before photobleaching. It is thus possible that similar mechanisms operated in our conditions. Raw fluorescence traces and superimposed fits used for the correction are shown in the insets. Details of how fits were generated and corrections performed are described in Materials and methods. In each tested fiber, the resulting depolarization-dependent increase in the FRET ratio R/R_0 (R_0 being the value of the ratio at –80 mV) was adjusted with a Boltzmann function. On average, Mermaid yielded a voltage dependence centered at a mid-value ($V_{0.5}$) of –38 mV (Table 1). Importantly, depolarizing and hyperpolarizing pulses of identical amplitude from –80 and 0 mV, respectively, generated symmetrical changes in the FRET ratio, with no sign of shift in the voltage sensitivity (Fig. 1 C). These results establish the efficiency and reliability of membrane voltage detection in isolated muscle fibers using the FRET signal from Mermaid.

FRET response of Rv-Mermaid: a Mermaid sensor adapted to accommodate the T306 SR targeting sequence

The next step was to express Mermaid fused to an SR-specific sequence. To target the SR membrane, we used a protein domain encompassing the 306 residues (T306) of the N-terminal end of triadin, an archetypal protein of the junctional SR (Rossi et al., 2014). To avoid having the T306 domain fused to mKOκ, we constructed reverse-Mermaid (Rv-Mermaid), in which the FRET couple is fused to the S1 segment of the VSD. Fusion of T306 on the S4 segment was then expected to ensure proper topology of the biosensor in the SR membrane (with the FRET couple facing the cytosol) in concurrence with the native topology of the T306 domain (Fig. S1). Rv-Mermaid also yielded an expression pattern consistent with t-tubule localization (Fig. 1 D), and this was confirmed by a FRET response qualitatively similar to that of Mermaid upon changes in membrane voltage (Fig. 1 E). However, Rv-Mermaid yielded a very negative midvoltage ($V_{0.5} \sim$ –70 mV; Fig. 1 F and Table 1), whereas the SR membrane voltage is presumed to be maintained at ∼0 mV (Somlyo et al., 1981). The variant Mermaid$^{D129E/Y235R}$ tested in *Xenopus* oocytes exhibits a midvoltage near +10 mV (H. Tsutsui, personal communication). Thus, to match Rv-Mermaid's

Figure 1. **Detection of t-tubule voltage changes with Mermaid and Rv-Mermaid in muscle fibers.** **(A and D)** Confocal pattern of the green fluorescence in muscle fibers expressing Mermaid and Rv-Mermaid, respectively. In each panel, the frame and graph on the right show a higher-magnification view together with the longitudinal profile of fluorescence within the white box. Expression of Mermaid and Rv-Mermaid yielded a transverse-banded pattern consistent with the proteins being present in the triadic region of the fibers. A schematic illustration of the structure of the proteins is shown at top. **(B and E)** Changes in mUKG (F_{500}, green) and mKOκ ($F_{>560}$, red) fluorescence and corresponding FRET ratio in response to the voltage-clamp protocol shown at top, from muscle fibers expressing Mermaid and Rv-Mermaid, respectively. In response to the voltage-clamp depolarizing steps from –80 mV, the detected changes in fluorescence (at 500 nm and >560 nm, upon 458-nm excitation) were consistent with voltage-dependent energy transfer between the two fluorophores mUKG and mKOκ, providing evidence for localization of Mermaid and Rv-Mermaid in the t-tubule membrane of the muscle fibers. Main traces in B and E have been corrected from time-dependent changes in fluorescence also observed when no voltage pulse was given. Raw fluorescence traces and superimposed fits used for the correction are shown in the insets. Details of how fits were generated and correction performed are described in Materials and methods. **(C)** Changes in Mermaid FRET ratio in response to depolarizing (left, black trace) and hyperpolarizing (right, blue trace) steps from –80 and 0 mV, respectively, in the same fiber. The graph at bottom shows the mean voltage dependence of the change in FRET ratio established from three fibers stimulated with a series of successive voltage-clamp depolarizing steps from –80 mV (black circles) and then with a series of successive hyperpolarizing steps from 0 mV (blue circles). FRET ratio values were normalized to the value R_0 at –80 mV. Step hyperpolarizing pulses from 0 mV generated symmetrical changes in the FRET ratio, with no detectable sign of shift in the voltage sensitivity. **(F)** Mean voltage dependence of the FRET response of Mermaid (n = 6) and Rv-Mermaid (n = 6) established using depolarizing steps from –80 mV. Error bars represent ± SEM.
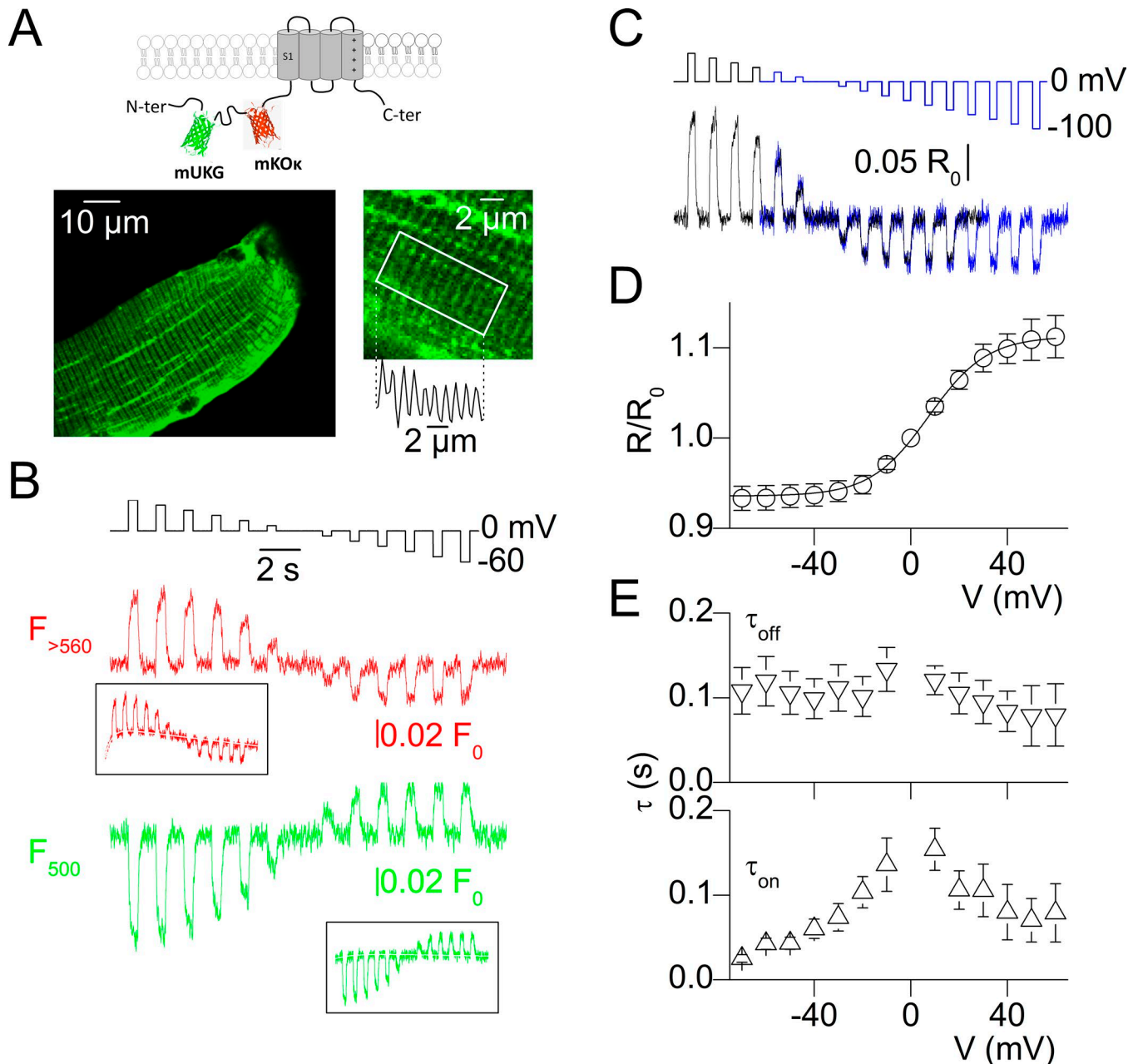
Figure 2. **FRET response of Rv-Mermaid^D129E/Y235R to changes in t-tubule membrane voltage applied from 0 mV. (A)** Schematic structure of Rv-Mermaid[D129E/Y235R] and its confocal triadic pattern in muscle fibers. **(B)** Changes in mUKG (F_{500}, green) and mKOκ ($F_{>560}$, red) fluorescence in response to the indicated voltage protocol. Insets show the corresponding raw records before correction for voltage-independent changes in fluorescence; the fit used for correction is shown in white. **(C)** Changes in the FRET ratio ($F_{>560}/F_{500}$) elicited in response to the pulse protocols shown at top. The black trace was from the fluorescent responses shown in B. **(D)** Mean voltage dependence of the FRET response measured with voltage pulses from 0 mV ($n = 6$). FRET ratio values were normalized to the value at 0 mV (R_0). **(E)** Mean voltage dependence of the time constant of change in FRET ratio at the onset (τ_{on}) and offset (τ_{off}) of the pulses. Error bars represent ± SEM.

$V_{0.5}$ with the resting SR voltage, we designed and expressed Rv-Mermaid^D129E/Y235R; this construct also exhibited a triadic localization (Fig. 2 A) and had a voltage sensitivity centered at +5 mV, as established from FRET responses to voltage-clamp pulses applied from 0 mV (Fig. 2, B–D; and Table 1). The rate of change in FRET ratio at the onset and offset of the pulses was approximated by a single exponential function: the "on" time constant yielded a bell-shaped voltage dependence with a maximum value of ~150 ms at +10 mV and a minimum value near

~25 ms, whereas the "off" time constant was rather independent from the pulse voltage (Fig. 2 E).

Evidence for mixed subcellular localization of Rv-Mermaid^D129E/Y235R

Interestingly, the FRET response from fibers expressing Rv-Mermaid^D129E/Y235R to depolarizing pulses applied from –80 mV qualitatively differed from that of Mermaid and Rv-Mermaid (Fig. 3). Indeed, depolarizing pulses to values ranging between –40 and

Table 1. Mean values for the parameters obtained from fitting a Boltzmann function to the FRET ratio (R/R$_0$) versus voltage data obtained with the different Mermaid constructs

Main subcellular distribution	Mermaid T-tubule (and SR?)	Rv-Mermaid T-tubule (and SR?)	Rv-Mermaid $^{D129E/Y235R}$ T-tubule and SR[a]	T306-Rv-Mermaid Junctional SR	T306-Rv-Mermaid $^{D129E/Y235R}$ Junctional SR
n	6	6	6	6	13
Max	0.17 ± 0.02	0.16 ± 0.02	0.17 ± 0.02	−0.075 ± 0.01	−0.06 ± 0.01
Min	0.99 ± 0.01	0.95 ± 0.01	0.93 ± 0.01	1	1
$V_{0.5}$ (mV)	−37.7 ± 7.1	−69.0 ± 4.1	5.45 ± 3.4	−26.4 ± 1.2	−26.2 ± 1.9
k (mV)	14.1 ± 0.46	14.9 ± 1.1	11.4 ± 0.5	5.5 ± 0.9	2.8 ± 0.9

Individual sets of data points from each fiber were fitted with the following expression: Max/{1 + exp[($V_{0.5}$ − V)/k]} + Min. Data are mean ± SEM.
[a]The voltage dependence was established from signals elicited by pulses from 0 mV.

−20 mV generated negative changes in FRET ratio (Fig. 3, A and B), whereas for more depolarized step levels, an additional component, similar to what was observed with Mermaid and Rv-Mermaid (Fig. 1), was present. Fig. 3 C shows the voltage dependence of the FRET ratio measured in six fibers, at the time of the end of each pulse during the protocol. There was variability, with some fibers exhibiting a very prominent negative change in FRET ratio at intermediate voltages (e.g., Fig. 3 C, triangles), whereas other ones had much less. We hypothesized that these complex responses resulted from two populations of Rv-Mermaid$^{-D129E/Y235R}$: one in the plasma/t-tubule membrane and the other in a distinct membrane compartment experiencing a distinct voltage change. Assuming that only the t-tubule population would respond to a voltage-clamp hyperpolarization, adding the FRET signal elicited by a pulse from −80 to 0 mV to the one elicited by a pulse from 0 to −80 mV unmasks the pure contribution of the non-t-tubule population (Fig. 3 D). Interestingly, when expressed in COS-7 cells, Rv-Mermaid$^{D129E/Y235R}$ appeared to localize both in the plasma membrane and, to some extent, in the ER. This is illustrated in Fig. S2, which shows the results of immunolabeling experiments using antibodies directed against either a Golgi or an ER marker protein. The depolarization-induced negative FRET signal in the muscle fibers may thus originate from the SR membrane.

FRET response of SR-targeted Mermaid biosensors to t-tubule membrane voltage changes

Mermaid biosensors fused to the T306 sequence were anticipated to specifically reveal electrical activity of the SR membrane during muscle fiber activation. In contrast with the other constructs tested in the present study that yielded a general distribution throughout the muscle fibers, the ones carrying the T306 targeting sequence exhibited a patchy expression pattern, with only one or a few localized spots of fluorescence, each in the vicinity of a nucleus. An example from a fiber expressing T306-Rv-Mermaid$^{D129E/Y235R}$ is shown in Fig. 4 A. This is reminiscent of what occurs when expressing RYR1 channels in the same model (Lefebvre et al., 2011). In addition, the fluorescence within the spots exhibited a typical triadic pattern, suggesting that we did succeed in targeting the junctional SR membrane with the T306 domain. This was confirmed by the ER localization of the construct using immunolabeling experiments in transfected COS-7

cells (Fig. S3). We cannot exclude that in the muscle fibers, some of the T306-fused Mermaid probes distributed to some extent in the nonjunctional SR membrane. However, considering the above expression features and the fact that use of a nonjunctional targeting sequence provided a very different expression pattern (see Fig. S5, A and D), we believe it is reasonable to assume that most of the T306-fused probes did reside in the junctional SR membrane. In muscle fibers, the FRET response of T306-Rv-Mermaid$^{D129E/Y235R}$ to voltage-clamp pulses was unique, as it had no sign, whatsoever, of a t-tubule contribution. In response to depolarizing pulses from −80 mV, the FRET ratio experienced only a decrease during the pulses. The amplitude of this drop increased with the t-tubule depolarization, with a voltage-dependence centered near −25 mV (Fig. 4, B and C; and Table 1). The time constant of onset of the signal decreased with the amplitude of depolarization within a 230–60-ms range, whereas the "off" time constant was voltage independent (Fig. 4 D). Because the construct was designed to have a membrane topology with the FRET couple facing the cytosol, the simplest interpretation is that this FRET signal corresponds to a negative polarization of the cytosolic face of the SR membrane with respect to the lumen. Assuming that the resting SR membrane voltage is 0 mV and that the sensor response is identical in the t-tubule membrane (Fig. 2 D) and in the SR membrane, then the maximum change in FRET ratio (6%; Fig. 4 C) would be consistent with an SR voltage change of at least 20 mV. Further evidence that the FRET response from T306-Rv-Mermaid$^{D129E/Y235R}$ to voltage-clamp depolarizing pulses is intimately linked to EC coupling is provided in Fig. S4, which shows that the FRET signal progressively collapses during a protocol of successive depolarizing pulses (Fig. S4 A), in concurrence with Ca^{2+} release. This occurs under these conditions because of voltage-dependent inactivation of EC coupling (Hodgkin and Horowicz, 1960). In response to hyperpolarizing pulses from 0 mV, T306-Rv-Mermaid$^{D129E/Y235R}$ also produces a small FRET response (Fig. S4 B), the onset of which coincides with t-tubule membrane repolarization to 0 mV and the amplitude of which increases as the hyperpolarization is made longer (Fig. S4 C), consistent with the FRET response being triggered upon recovery of EC coupling from inactivation.

To confirm that the change in fluorescence detected by T306-Rv-Mermaid$^{D129E/Y235R}$ upon EC coupling activation did result
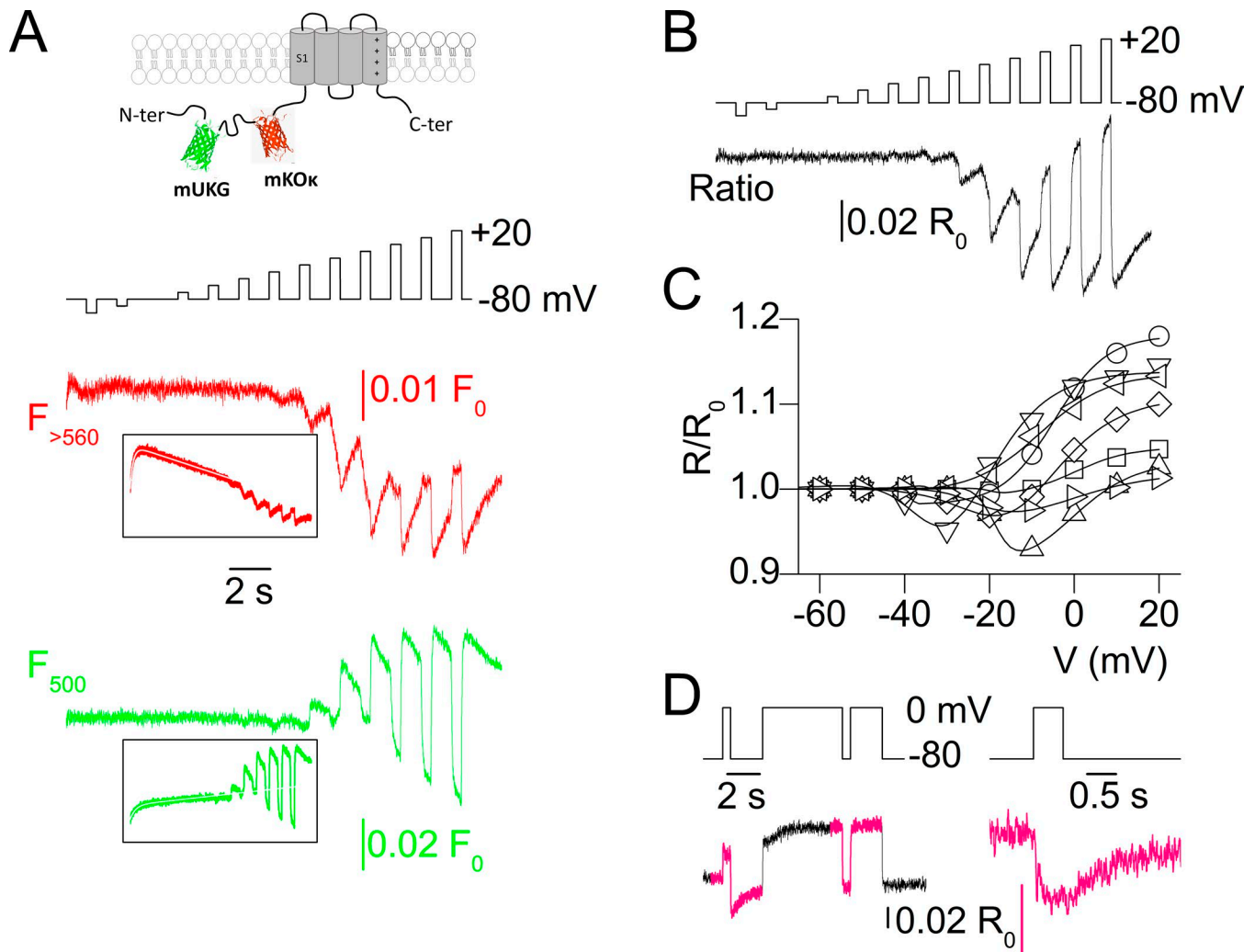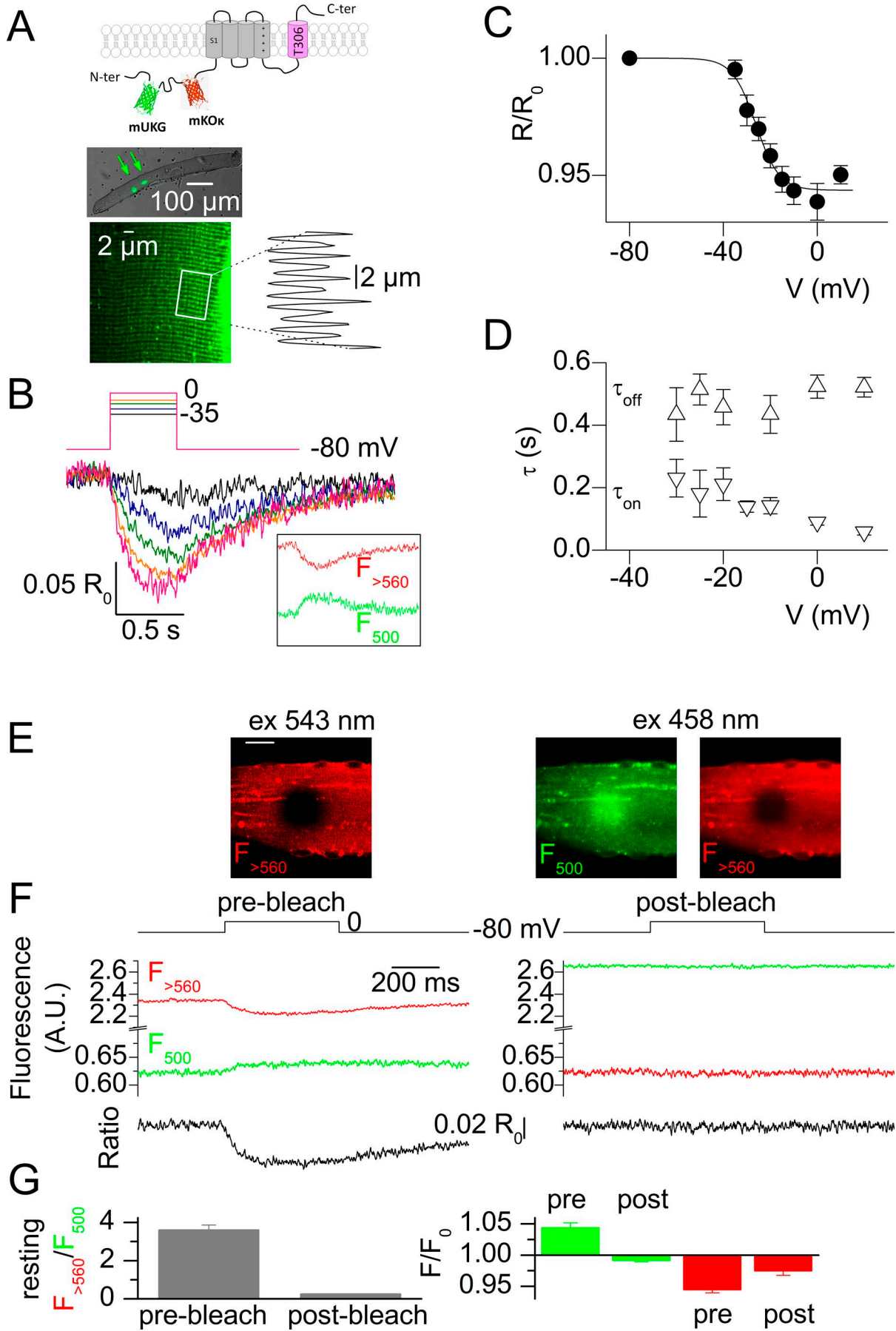
Figure 3. **Complex response of Rv-Mermaid[D129E/Y235R] to t-tubule membrane depolarization from −80 mV. (A)** Schematic structure of Rv-Mermaid[D129E/Y235R] and the changes in mUKG and mKOκ fluorescence in response to the indicated voltage-clamp pulse protocol. Insets show the corresponding raw records before correction for voltage-independent changes in fluorescence; the fit used for correction is shown in white. **(B)** FRET ratio calculated from the fluorescent traces shown in A. **(C)** Voltage dependence of the end-pulse FRET ratio measured in response to the pulse protocol shown in A and B. Datasets are from seven muscle fibers, six of which were the ones used to generate mean values shown in Fig. 2 D. **(D)** Asymmetrical response to a depolarization from −80 mV compared with a hyperpolarization from 0 mV. Left: The FRET ratio (bottom trace) was measured in response to the pulse protocol shown at top. The pink portions of traces were synchronized and summed to produce the pink trace on the right.

from a change in FRET, we performed acceptor photobleaching experiments. The protocol was first tested on the resting fluorescence from fibers expressing a non-SR-targeted Mermaid construct. Fig. 4 E shows *x,y* fluorescence frames from a muscle fiber expressing Rv-Mermaid[D129E/Y235R]. A square region in the middle of the fiber was scanned during several minutes at 543 nm with high laser power until substantial bleaching occurred (Fig. 4 E, left). As expected, upon subsequent excitation at 458 nm in FRET detection configuration, extinction of the acceptor fluorescence was accompanied by dequenching of the donor in the photobleached region (Fig. 4 E, right). Fig. 4 F illustrates the effect of acceptor photobleaching on the changes in fluorescence detected in response to a 0.5-s-long depolarizing pulse from −80 to 0 mV in FRET configuration (458-nm excitation) from a fiber expressing T306-Rv-Mermaid[D129E/Y235R]; traces on the left and right were recorded before and after photobleaching

with 543-nm light, respectively. Again, photobleaching induced an increase and decrease in the resting donor and acceptor fluorescence, respectively, and this was accompanied by a loss of the transient changes in fluorescence triggered by the pulse and of the corresponding change in FRET ratio. Fig. 4 G shows mean values for the resting fluorescence ratio (left) and the relative changes in F_{500} and $F_{>560}$ fluorescence triggered by a strong depolarizing pulse, from five fibers expressing T306-Rv-Mermaid[D129E/Y235R] and tested under the same conditions as described in Fig. 4 F. The photobleaching-induced loss of pulse-triggered changes in fluorescence establishes that these changes (and the corresponding change in ratio), result from FRET.

In an attempt to confirm the occurrence of an SR membrane–specific voltage-dependent FRET signal, we tested an alternative SR-targeted probe, ER-Mermaid2[D129E], which makes use of a CFP–YFP FRET pair and of an arginine-based targeting sequence (ER;

Sanchez et al.
Electrical activity of the reticulum membrane

Journal of General Physiology
https://doi.org/10.1085/jgp.201812035

1170

A

C

B

D

ex 543 nm   ex 458 nm

E

pre-bleach   0   -80 mV   post-bleach

F

G

Sharma et al., 2010) expected to allow expression throughout the entire SR membrane. ER-Mermaid2^{D129E} indeed exhibited a fluorescence pattern consistent with widespread expression in the SR membrane (Fig. S5, A and D; and Fig. S6). More specifically, ER-Mermaid2^{D129E} exhibited a transverse striated pattern, but in contrast to the other constructs, the longitudinal fluorescence profile was composed of successive "single" bands separated by 2 µm (Fig. S5 D, green trace on the right corresponding to the fluorescence profile along the white box). Imaging of the t-tubule network with di-8-anepps (Fig. S5 D, red image and corresponding longitudinal profile along the same white box) indicated that the protein was concentrated around the Z line, consistent with the standard expression pattern of nonjunctional SR proteins (Sorrentino, 2011). However, ER-Mermaid2^{D129E} responded to voltage-clamp steps from 0 mV (Fig. S5, B and C), demonstrating presence in the t-tubule membrane, and thus indicating that the ER signal was not as strong as T306 to ensure exclusive SR localization. Although, in response to depolarizing pulses from −80 mV, ER-Mermaid2^{D129E} responded by a mixed signal (Fig. S5, E and F) similar to that observed with Rv-Mermaid$^{-D129E/Y235R}$ (Fig. 3), thus consistent with a response from probe molecules in the SR membrane, the nonstrict SR membrane targeting of ER-Mermaid2^{D129E} was very limiting and we thus did not pursue investigations with this probe.

T306-Rv-Mermaid provides a FRET response similar to that of T306-Rv-Mermaid$^{D129E/Y235R}$ despite its distinct range of voltage sensitivity

To further characterize the SR membrane–confined FRET change detected by Rv-Mermaid$^{D129E/Y235R}$ upon Ca^{2+} release activation, we also tested the response of T306-Rv-Mermaid. Because the voltage sensitivity of Rv-Mermaid is centered near a much more negative value than that of Rv-Mermaid$^{D129E/Y235R}$ (Figs. 1 and 2), very distant from the presumed resting SR membrane voltage, we expected a much reduced FRET response, if any. Fig. 5 A shows that T306-Rv-Mermaid exhibited a patchy expression pattern similar to the one of T306-Rv-Mermaid$^{D129E/Y235R}$. However, in response to depolarizing pulses from −80 mV, the FRET ratio also experienced a voltage-dependent decrease during the pulses, the amplitude and voltage dependence of which were very similar to those of T306-Rv-Mermaid$^{D129E/Y235R}$ (Fig. 5, B and C; and Table 1). Considering the distinct range of sensitivity to voltage of the two probes, this result was unexpected.

pH sensitivity of the FRET signal from Mermaid biosensors

The similarity between the FRET response of T306-Rv-Mermaid and T306-Rv-Mermaid$^{D129E/Y235R}$ makes it questionable whether this signal actually witnesses a change in SR membrane voltage. Because our standard experimental conditions make use of a large concentration of EGTA inside the muscle fibers to block contraction, a slight change in cytosolic pH is expected during Ca^{2+} release, because Ca^{2+} binding to EGTA releases protons. Although the Mermaid fluorescent proteins were initially designed to be pH resistant (Tsutsui et al., 2008), we tested whether a change in pH could affect the FRET signal using muscle fibers treated with the H$^+$ ionophore nigericin. Under these conditions, we found that the FRET signal from T306-Rv-Mermaid$^{D129E/Y235R}$ was very sensitive to pH. This is illustrated in Fig. 6 A, which shows fluorescence levels and the corresponding FRET ratio from an intact fiber challenged by successive changes in pH in the 6–7.5 range. Fig. 6 B shows values for the change in FRET ratio experienced by five nigericin-treated muscle fibers expressing T306-Rv-Mermaid$^{D129E/Y235R}$, upon various changes in pH. The FRET ratio was expressed either as R/R_{pH7} or $R/R_{pH7.2}$. Results clearly establish the sensitivity to pH of the FRET signal.

FRET response of SR-targeted Mermaid biosensors to t-tubule membrane voltage changes under conditions limiting cytosolic changes in pH

To circumvent the pH change caused by Ca^{2+} binding to EGTA, we performed experiments in the presence of BAPTA instead, which exhibits much less pH sensitivity (Tsien, 1980). Under these conditions, hardly any change in the T306-Rv-Mermaid$^{D129E/Y235R}$ FRET signal could be detected after depolarizing pulses. This is illustrated in Fig. 7 A, which shows a family of FRET ratio traces collected while applying 0.5-s-long depolarizing pulses between −30 and +10 mV. Loss of the negative FRET signal was not caused by suppression of Ca^{2+} release, as fibers equilibrated with BAPTA still yielded robust voltage-activated Ca^{2+} transients, though of smaller amplitude than in the presence of EGTA. For instance, a 500-ms-long voltage-clamp depolarization applied to seven fibers equilibrated with EGTA and four fibers equilibrated with BAPTA triggered a rhod-2 Ca^{2+} transient of mean initial peak F/F_0 amplitude of 3.5 ± 0.4 and 1.7 ± 0.2, respectively (Fig. 7 B). In Fig. 7 A, the trace shown in the inset corresponds to the mean response to 6–10 0.5-s-long pulses to voltages ranging between +10 and +40 mV from four fibers expressing T306-Rv-Mermaid$^{D129E/Y235R}$; traces from each fiber were averaged, and the

---

Figure 4.   **FRET response of T306-Rv-Mermaid$^{D129E/Y235R}$ during Ca^{2+} release. (A)** Patchy expression (regions pointed by green arrows) and triadic confocal pattern (bottom image and associated graph showing the longitudinal fluorescence profile along the white box) of T306-Rv-Mermaid$^{D129E/Y235R}$ in muscle fibers. Schematic structure of the protein is shown at top. **(B)** Changes in T306-Rv-Mermaid$^{D129E/Y235R}$ FRET ratio in response to the indicated voltage-clamp depolarizing pulses. Inset shows the fluorescent traces in response to the pulse from −80 to −10 mV. **(C)** Mean voltage dependence of the peak amplitude of the drop in FRET ratio measured in response to single 0.5-s-long pulses from −80 mV. For this, successive single depolarizing pulses of increasing amplitude were applied, separated by a time interval of 30 s. Data points are mean values from several fibers ranging from a minimum of seven and a maximum of 13. **(D)** Mean voltage dependence of the time constant of change in FRET ratio at the onset (τ_{on}) of the depolarizing pulses and upon return (τ_{off}) to the holding value of −80 mV. **(E)** Acceptor photobleaching of the resting fluorescence from a fiber expressing Rv-Mermaid$^{D129E/Y235R}$: x,y fluorescence frames after photobleaching of a square region in the middle of the fiber with excitation light at 543 nm. Bar, 20 µm. **(F)** Effect of acceptor photobleaching (postbleach) on the changes in fluorescence detected in response to a depolarizing pulse from −80 to 0 mV in FRET configuration (458-nm excitation) from a fiber expressing T306-Rv-Mermaid$^{D129E/Y235R}$. **(G)** Mean values for the resting fluorescence ratio (left) and the relative changes in F_{500} and $F_{>560}$ fluorescence (right) triggered by a strong depolarizing pulse, from five fibers expressing T306-Rv-Mermaid$^{D129E/Y235R}$. Error bars represent ± SEM.
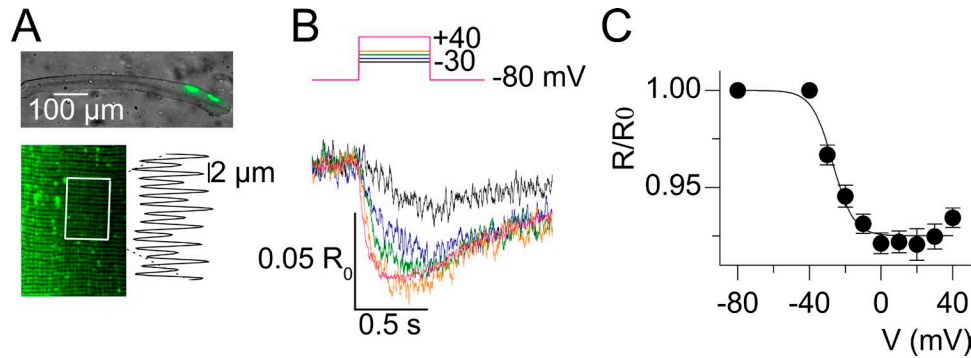

Figure 5. FRET response of T306-Rv-Mermaid during Ca²⁺ release. (A) Patchy expression and triadic confocal pattern (bottom image and associated trace showing the longitudinal fluorescence profile along the white box) of T306-Rv-Mermaid in muscle fibers. **(B)** Changes in T306-Rv-Mermaid FRET ratio in response to the indicated voltage-clamp depolarizing pulses. **(C)** Mean voltage dependence of the peak amplitude of the drop in FRET ratio measured in response to single 0.5-s-long pulses from –80 mV. For this, successive single depolarizing pulses of increasing amplitude were applied, separated by a time interval of 30 s. Data points are mean values from six fibers. Error bars represent ± SEM.

mean was calculated from the four mean traces. This revealed a slight positive change in the ratio that did not exceed 0.015 R_0. According to the calibrated FRET response in Fig. 2 D, this could correspond to a <10 mV depolarization. Alternatively, according to the fit shown in Fig. 6 B, it could correspond to an alkalization of ~0.06 pH units. We also attempted to measure the FRET response in the absence of exogenous intracellular Ca²⁺ buffer, using the contraction blocker BTS in the extracellular medium. However, under our standard conditions of stimulation with hundreds of milliseconds–long voltage-clamp pulses, BTS never completely eliminated contraction, precluding measurements in response to large pulses that maximally activate Ca²⁺ release. Still, measurements in response to 0.5-s-long pulses up to –25 or –20 mV never elicited any negative FRET response. Instead, a slight positive change in the ratio was observed, as illustrated in Fig. 7 C, which shows FRET ratio traces from a fiber expressing T306-Rv-Mermaid^D129E/Y235R challenged by pulses up to –20 mV

in the presence of BTS. Under these conditions, data from three fibers gave a mean change in FRET ratio of 0.03 ± 0.002 R_0. In our hands, BTS proved much more effective to block contraction triggered by trains of action potentials. We thus took measurements of FRET signals from T306-Rv-Mermaid constructs in such conditions. The response of two distinct fibers expressing T306-Rv-Mermaid^D129E/Y235R to a train of action potentials is shown in Fig. 7 (D and E); in Fig. 7 D, the fiber was equilibrated with our standard EGTA-containing solution in the voltage-clamp pipette, whereas in Fig. 7 E, no EGTA was used inside the pipette, but BTS was present in the extracellular solution. Results further confirm the EGTA dependence of the negative FRET signal upon EC coupling activation and the presence of a small FRET signal of opposite direction in the absence of EGTA. Fig. 7 F illustrates the fact that, in the absence of EGTA (and presence of BTS), T306-Rv-Mermaid also responded by a positive change in FRET of amplitude similar to the one observed with T306-Rv-Mermaid^D129E/Y235R,
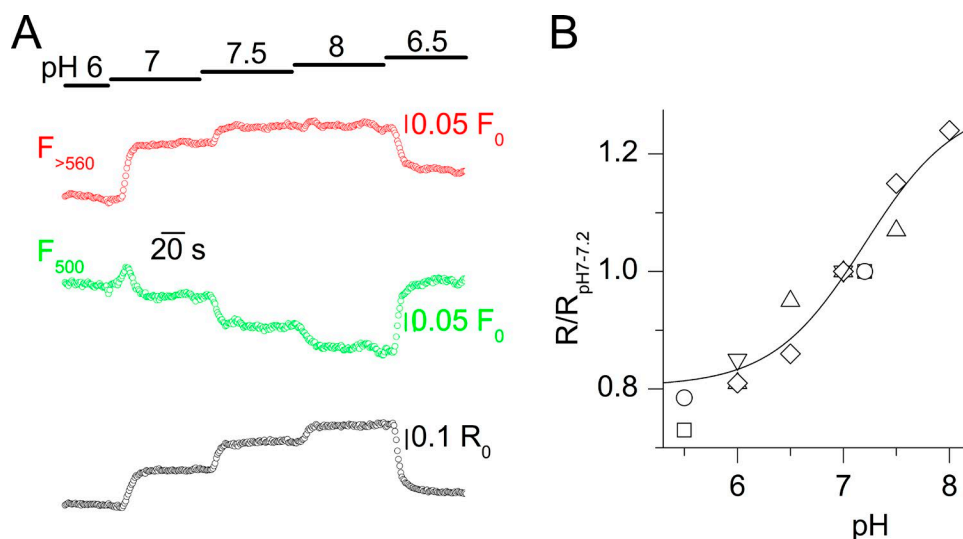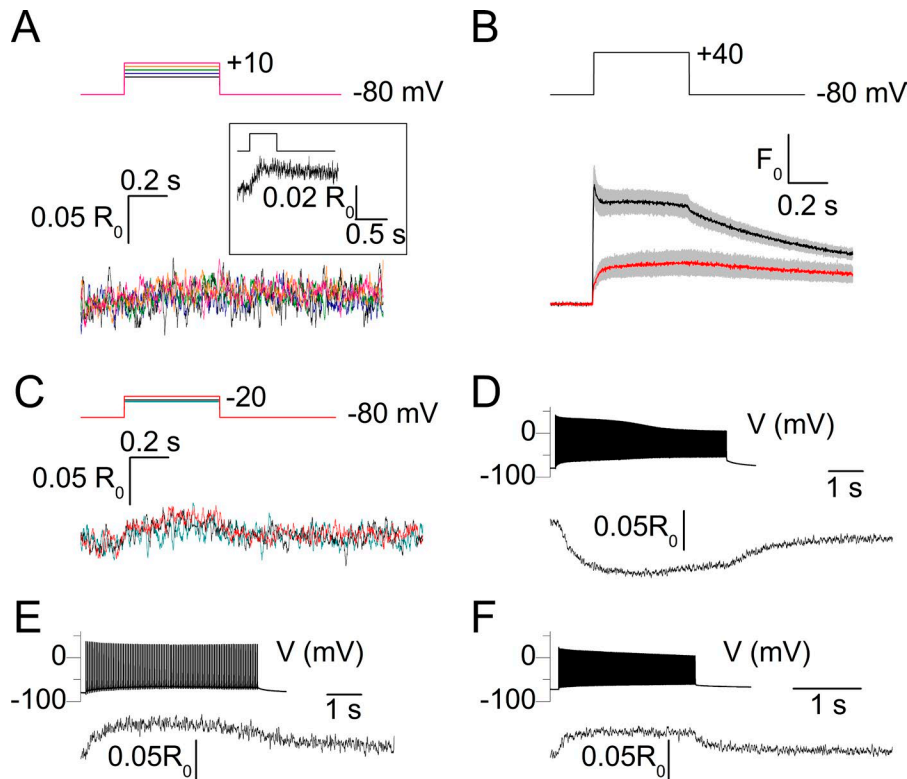

Figure 6. pH sensitivity of the FRET response from T306-Rv-Mermaid during Ca²⁺ release. (A) Changes in fluorescence and in the corresponding FRET ratio in response to extracellular changes in pH in the presence of nigericin, in a muscle fiber expressing T306-Rv-Mermaid^D129E/Y235R. **(B)** Change in FRET ratio from five nigericin-treated muscle fibers expressing T306-Rv-Mermaid^D129E/Y235R, upon changes in pH. Each symbol corresponds to a different fiber. The continuous line shows the result from fitting a Hill equation to the data shown as triangles, inverted triangles, and diamonds.

Sanchez et al.
Electrical activity of the reticulum membrane

Journal of General Physiology
https://doi.org/10.1085/jgp.201812035

1173

Figure 7. **FRET response of T306-Rv-Mermaid**[D129E/Y235R] **and T306-Rv-Mermaid during Ca²⁺ release in the absence of intracellular EGTA. (A)** FRET response to 0.5-s-long voltage-clamp depolarizing pulses to values ranging between –30 and +10 mV from a muscle fiber expressing T306-Rv-Mermaid[D129E/Y235R], equilibrated in the presence of intracellular BAPTA. The inset shows the mean response from four fibers to large depolarizing pulses in the same condition (see text for details). Successive single depolarizing pulses were separated by a time interval of 30 s. **(B)** Mean rhod-2 cytosolic Ca²⁺ transient elicited by a depolarizing pulse from –80 to +40 mV in seven fibers equilibrated with intracellular EGTA (black trace) and four fibers equilibrated with intracellular BAPTA (red trace). Gray shading corresponds to SEM. **(C)** FRET response to 0.5-s-long depolarizing voltage-clamp pulses to –35, –30, and –20 mV from a muscle fiber expressing T306-Rv-Mermaid[D129E/Y235R] in the presence of extracellular BTS. Successive single depolarizing pulses were separated by 30 s. **(D)** FRET response of a muscle fiber expressing T306-Rv-Mermaid[D129E/Y235R], equilibrated with intracellular EGTA, to a train of action potentials generated at 100 Hz. **(E)** FRET response of a muscle fiber expressing T306-Rv-Mermaid[D129E/Y235R], equilibrated without intracellular EGTA and in the presence of extracellular BTS, to a train of action potentials generated at 20 Hz. **(F)** FRET response of a fiber expressing T306-Rv-Mermaid, equilibrated without intracellular EGTA and in the presence of extracellular BTS, to a train of action potentials at 100 Hz.

which, considering the very different midvoltage sensitivities of the two probes, tends to exclude that this signal corresponds to an SR membrane voltage change.

Discussion

The question of whether the membrane of the reticulum experiences voltage changes during cellular activity was experimentally addressed more than 30 yr ago in isolated frog muscle fibers, through detection of optical retardation signals and through the use of potentiometric dyes (Baylor and Oetliker, 1975, 1977; Vergara et al., 1978; Kovács et al., 1983; Baylor et al., 1984). However, these studies did not lead to coherent results, and no further attempt was made. In the same period, results from electron probe x-ray microanalysis of ion distribution and movements across the SR membrane established the currently admitted view, according to which there is no large voltage gradient across the SR membrane at rest or during Ca²⁺ release (Somlyo et al., 1977, 1981, 1985). This view was corroborated by the identification and characterization of K⁺ and Cl⁻ channels in the SR membrane that could participate to the counter-Ca²⁺ release current necessary to maintain the SR membrane voltage clamped near its resting value during Ca²⁺ release (Labarca and Miller, 1981; Rousseau et al., 1988; Abramcheck and Best, 1989; Wang and Best, 1994; Kourie et al., 1996; Yazawa et al., 2007). Conversely, it was also proposed that need for these channels may be limited, as the

open RYR could itself carry most of the necessary countercurrent (Gillespie and Fill, 2008; Guo et al., 2013). In this context, the now-available option of targeting a genetically engineered voltage-sensitive fluorescent tool to the SR membrane offered a unique opportunity to experimentally settle this point.

Mermaid biosensors in the SR membrane are sensitive to cytosolic acidification induced upon Ca²⁺ binding to EGTA
In the present conditions, Mermaid constructs devoid of SR targeting sequence were present in the plasma/t-tubule membrane of the transfected muscle fibers, allowing quantitative characterization of the properties of the voltage-induced changes in FRET. Use of the T306 sequence then proved successful to target the constructs to the junctional SR membrane, as no more plasma/t-tubule membrane–related FRET change was detected in fibers expressing the T306 constructs. Under these conditions, use of Rv-Mermaid and Rv-Mermaid[D129E/Y235R], yielding distinct voltage sensitivity (centered near –70 and 0 mV, respectively), was anticipated to allow differentiation of any EC-coupling activated FRET signal caused by an actual change in SR membrane voltage from a change in any other parameter that could affect FRET. Indeed, the two constructs should provide a response of very different amplitude to a given voltage change, if voltage were the only parameter affecting FRET. This was obviously not the case: both constructs provided very similar responses in the different conditions tested. In the presence of intracellular EGTA,

they responded by a change in FRET consistent with sensitivity of the probes to acidification of the cytosolic face of the SR membrane. Because the response was very similar for the two probes, pH sensitivity was not a consequence of the mutations. A cytosolic pH change has been well documented in frog muscle fibers loaded with EGTA, where it was used to measure and quantify the EC coupling-activated cytosolic Ca^{2+} transients using the EGTA-phenol red method (Pape et al., 1995, 1998, 2002; Pizarro and Ríos, 2004). Under conditions of voltage-clamp stimulation similar to the ones used here, Pizarro and Ríos (2004) reported maximum cytosolic levels of increase in $[H^+]$ of 0.2–0.3 μM, which would translate into a change of 0.6–0.8 pH units. According to our calibration in nigericin-treated fibers (Fig. 6), the maximum decrease in FRET ratio (6%, Fig. 4) evoked by a large depolarizing pulse in fibers expressing Rv-Mermaid$^{D129E/Y235R}$ would correspond to a change in pH from 7.2 to 6.97. One interesting point is that no sign of cytosolic acidification was detected with the non-SR-targeted Mermaid constructs (assuming that the mixed response of Rv-Mermaid$^{D129E/Y235R}$ was caused by its mixed plasma/SR membrane localization). Yet, in both the plasma membrane and the SR membrane, the topology of the probe proteins yields the FRET pair facing the cytosol, this concurring with the native topology of the T306 domain for the SR-targeted forms. Then, absence of "pH response" of the probes residing in the plasma/t-tubule membrane has to indicate that the pH change detected in the vicinity of the SR membrane spared the cytosolic face of the t-tubule membrane. This is somewhat inconsistent with calculations by Pape et al. (1995), which suggest that, in the presence of a large concentration of intracellular EGTA, changes in $[H^+]$ remain substantial hundreds of nanometers away from a single Ca^{2+}-releasing site and that even in the case of Ca^{2+} release from many release channels, a substantial $[H^+]$ gradient near the Ca^{2+} release sites is unlikely. In contrast, our results suggest that a change in cytosolic pH can be detected by probes in the junctional SR membrane but not by probes in the t-tubule membrane. Because, in fast-twitch muscle fibers, the majority of the t-tubule network is involved in junctional contact with the SR (Franzini-Armstrong et al., 1988), most of the Mermaid probes in the t-tubule membrane should reside less than 20 nm (Felder et al., 2002) away from the Ca^{2+} release channels. Thus, they would be expected to sense as well the pH changes caused by H^+ release from EGTA. At present, we do not have a clear explanation for this inconsistency. An alternative explanation could be that the FRET response to voltage-clamp depolarizing pulses of Mermaid and Rv-Mermaid in the t-tubule membrane was, to some extent, corrupted by a pH-dependent component that remained masked by the voltage-dependent component, because of the negative voltage sensitivity of these two probes. This is unlikely, however; given the substantial amplitude of the acidification-induced FRET change and the fact that its off time constant (Fig. 4 D) is ∼5 times slower than the off time constant of the signal from probes in the t-tubule membrane (Fig. 2 E), a pH-dependent component of the FRET signal in the t-tubule membrane would have strongly contaminated the voltage-dependent FRET signal from Mermaid and Rv-Mermaid. Furthermore, the symmetrical FRET response of Mermaid to depolarizing and hyperpolarizing pulses of identical amplitude (Fig. 1 C) also argues against this possibility. It may

be speculated that the negative FRET response of SR-targeted Mermaid probes is caused by Ca^{2+} sensitivity of the FRET signal. However, that this response was not present in the absence of EGTA strongly argues against this possibility, because in that condition, if changed, the Ca^{2+} transient should be larger than in the presence of EGTA. Altogether, our results indicate difficulties in using Mermaid probes as local voltage detectors where robust and rapid changes in pH take place. However, they also point out the reliability of the T306 target signal to convey a signal that is restricted to the intimate cytosolic environment of the SR membrane.

No evidence for an SR voltage change during muscle fiber activation under conditions limiting cytosolic changes in pH

In the absence of intracellular EGTA (either replaced by BAPTA or in the presence of the contraction blocker BTS), there was no sign of negative change in FRET ratio from T306-Rv-Mermaid constructs during activation of Ca^{2+} release. Upon Ca^{2+} binding, BAPTA releases much fewer protons than EGTA (Fénelon and Pape, 2002), which thus further supports the pH nature of the negative FRET signal observed in the presence of EGTA. However, BAPTA yields substantially higher affinity and faster kinetics than EGTA (Pape et al., 2002; Sztretye et al., 2011). Thus, corresponding disappearance of the negative FRET signal (Fig. 7 A) may be speculated to result from circumvention of a positive feedback of the released Ca^{2+} ions on either Ca^{2+} release activity itself or on other Ca^{2+}-dependent channels implicated in SR membrane voltage control (e.g., Pitt et al., 2010). Alternatively, large concentrations of BAPTA may also be suspected to have a deleterious pharmacological effect on Ca^{2+} release (Pape et al., 2002), which could also contribute to attenuate the negative FRET signal. The fact that robust Ca^{2+} transients were still elicited in the presence of BAPTA indicates that disappearance of the negative FRET signal did not result from failing SR Ca^{2+} release. Furthermore, the fact that experiments in the presence of BTS also showed no sign of negative FRET signal from the SR membrane–targeted probes tends to definitely eliminate the option that this signal witnesses an SR membrane voltage change.

Instead, in the absence of EGTA, both the native and the D129E/Y235R form of T306-Rv-Mermaid responded by a small increase in the FRET ratio that, again, can hardly be thought to result from an SR membrane voltage change, considering the differing midvoltage sensitivity of the two probes. The mean change in FRET ratio recorded in response to a voltage-clamp pulse to −20 mV was ∼0.03 R_0, and a response of similar amplitude was recorded in response to a train of action potentials (Fig. 7 E). According to the pH dependence of Rv-Mermaid$^{D129E/Y235R}$ (Fig. 6), this change would correspond to a cytosolic alkalization from 7.2 to 7.31. A small alkalization of the cytosol was previously reported to occur in conjunction with Ca^{2+} release in frog muscle fibers, consistent with a proton flux from the cytosol into the SR (Baylor et al., 1982; Hollingworth and Baylor, 1990; Pape et al., 1990). It is thus possible that in our conditions, in the absence of intracellular EGTA, the FRET response of T306-Rv-Mermaid constructs reveals the same process.

In conclusion, voltage-sensitive Mermaid probes targeted to the SR membrane of intact muscle fibers exhibit changes in

FRET upon activation of Ca^{2+} release that most likely report local changes in pH occurring in the vicinity of the SR membrane during the process. Results provide no evidence for additional FRET changes that would be caused by a substantial variation of SR membrane voltage during muscle EC coupling.

Acknowledgments

References

Abramcheck, C.W., and P.M. Best. 1989. Physiological role and selectivity of the in situ potassium channel of the sarcoplasmic reticulum in skinned frog skeletal muscle fibers. *J. Gen. Physiol.* 93:1–21. https://doi.org/10.1085/jgp.93.1.1

Armstrong, C.M., and B. Hille. 1998. Voltage-gated ion channels and electrical excitability. *Neuron.* 20:371–380. https://doi.org/10.1016/S0896-6273(00)80981-2

Baylor, S.M., and H. Oetliker. 1975. Birefringence experiments on isolated skeletal muscle fibres suggest a possible signal from the sarcoplasmic reticulum. *Nature.* 253:97–101. https://doi.org/10.1038/253097a0

Baylor, S.M., and H. Oetliker. 1977. Birefringence signals from surface and t-system membranes of frog single muscle fibres. *J. Physiol.* 264:199–213. https://doi.org/10.1113/jphysiol.1977.sp011663

Baylor, S.M., W.K. Chandler, and M.W. Marshall. 1982. Optical measurements of intracellular pH and magnesium in frog skeletal muscle fibres. *J. Physiol.* 331:105–137. https://doi.org/10.1113/jphysiol.1982.sp014367

Baylor, S.M., W.K. Chandler, and M.W. Marshall. 1984. Calcium release and sarcoplasmic reticulum membrane potential in frog skeletal muscle fibres. *J. Physiol.* 348:209–238. https://doi.org/10.1113/jphysiol.1984.sp015106

Berridge, M.J. 1993. Inositol trisphosphate and calcium signalling. *Nature.* 361:315–325. https://doi.org/10.1038/361315a0

Bertrán, G.C., C. D'Alessio, and B.A. Kotsias. 1995. [Ion channels in nonexcitable cells]. *Medicina (B. Aires).* 55:449–456.

Chu, J., R.D. Haynes, S.Y. Corbel, P. Li, E. González-González, J.S. Burg, N.J. Ataie, A.J. Lam, P.J. Cranfill, M.A. Baird, et al. 2014. Non-invasive intravital imaging of cellular differentiation with a bright red-excitable fluorescent protein. *Nat. Methods.* 11:572–578. https://doi.org/10.1038/nmeth.2888

Felder, E., F. Protasi, R. Hirsch, C. Franzini-Armstrong, and P.D. Allen. 2002. Morphology and molecular composition of sarcoplasmic reticulum surface junctions in the absence of DHPR and RyR in mouse skeletal muscle. *Biophys. J.* 82:3144–3149. https://doi.org/10.1016/S0006-3495(02)75656-7

Fénelon, K., and P.C. Pape. 2002. Recruitment of Ca(2+) release channels by calcium-induced Ca(2+) release does not appear to occur in isolated Ca(2+) release sites in frog skeletal muscle. *J. Physiol.* 544:777–791. https://doi.org/10.1113/jphysiol.2002.026658

Fink, R.H., and C. Veigel. 1996. Calcium uptake and release modulated by counter-ion conductances in the sarcoplasmic reticulum of skeletal muscle. *Acta Physiol. Scand.* 156:387–396. https://doi.org/10.1046/j.1365-201X.1996.212000.x

Franzini-Armstrong, C., D.G. Ferguson, and C. Champ. 1988. Discrimination between fast- and slow-twitch fibres of guinea pig skeletal muscle using the relative surface density of junctional transverse tubule membrane. *J. Muscle Res. Cell Motil.* 9:403–414. https://doi.org/10.1007/BF01774067

Gillespie, D., and M. Fill. 2008. Intracellular calcium release channels mediate their own countercurrent: The ryanodine receptor case study. *Biophys. J.* 95:3706–3714. https://doi.org/10.1529/biophysj.108.131987

Guo, T., A. Nani, S. Shonts, M. Perryman, H. Chen, T. Shannon, D. Gillespie, and M. Fill. 2013. Sarcoplasmic reticulum K(+; TRIC) channel does not carry essential countercurrent during Ca(2+) release. *Biophys. J.* 105:1151–1160. https://doi.org/10.1016/j.bpj.2013.07.042

Hodgkin, A.L., and P. Horowicz. 1960. Potassium contractures in single muscle fibres. *J. Physiol.* 153:386–403. https://doi.org/10.1113/jphysiol.1960.sp006541

Hodgkin, A.L., and A.F. Huxley. 1952. A quantitative description of membrane current and its application to conduction and excitation in nerve. *J. Physiol.* 117:500–544. https://doi.org/10.1113/jphysiol.1952.sp004764

Hollingworth, S., and S.M. Baylor. 1990. Changes in phenol red absorbance in response to electrical stimulation of frog skeletal muscle fibers. *J. Gen. Physiol.* 96:473–491. https://doi.org/10.1085/jgp.96.3.473

Jacquemond, V. 1997. Indo-1 fluorescence signals elicited by membrane depolarization in enzymatically isolated mouse skeletal muscle fibers. *Biophys. J.* 73:920–928. https://doi.org/10.1016/S0006-3495(97)78124-4

Kourie, J.I., D.R. Laver, P.R. Junankar, P.W. Gage, and A.F. Dulhunty. 1996. Characteristics of two types of chloride channel in sarcoplasmic reticulum vesicles from rabbit skeletal muscle. *Biophys. J.* 70:202–221. https://doi.org/10.1016/S0006-3495(96)79564-4

Kovács, L., R.A. Schümperli, and G. Szücs. 1983. Comparison of birefringence signals and calcium transients in voltage-clamped cut skeletal muscle fibres of the frog. *J. Physiol.* 341:579–593. https://doi.org/10.1113/jphysiol.1983.sp014825

Kuum, M., V. Veksler, J. Liiv, R. Ventura-Clapier, and A. Kaasik. 2012. Endoplasmic reticulum potassium-hydrogen exchanger and small conductance calcium-activated potassium channel activities are essential for ER calcium uptake in neurons and cardiomyocytes. *J. Cell Sci.* 125:625–633. https://doi.org/10.1242/jcs.090126

Labarca, P.P., and C. Miller. 1981. A K+-selective, three-state channel from fragmented sarcoplasmic reticulum of frog leg muscle. *J. Membr. Biol.* 61:31–38. https://doi.org/10.1007/BF01870750

Lefebvre, R., C. Legrand, E. González-Rodríguez, L. Groom, R.T. Dirksen, and V. Jacquemond. 2011. Defects in Ca²⁺ release associated with local expression of pathological ryanodine receptors in mouse muscle fibres. *J. Physiol.* 589:5361–5382. https://doi.org/10.1113/jphysiol.2011.216408

Martonosi, A.N. 1996. Structure-function relationships in the Ca(2+)-ATPase of sarcoplasmic reticulum: Facts, speculations and questions for the future. *Biochim. Biophys. Acta.* 1275:111–117. https://doi.org/10.1016/0005-2728(96)00059-X

Meissner, G. 1994. Ryanodine receptor/Ca²⁺ release channels and their regulation by endogenous effectors. *Annu. Rev. Physiol.* 56:485–508. https://doi.org/10.1146/annurev.ph.56.030194.002413

Oetliker, H. 1989. Energetical considerations related to calcium release from the sarcoplasmic reticulum in skeletal muscle. *Biomed. Biochim. Acta.* 48:S313–S318.

Pape, P.C., M. Konishi, S. Hollingworth, and S.M. Baylor. 1990. Perturbation of sarcoplasmic reticulum calcium release and phenol red absorbance transients by large concentrations of fura-2 injected into frog skeletal muscle fibers. *J. Gen. Physiol.* 96:493–516. https://doi.org/10.1085/jgp.96.3.493

Pape, P.C., D.S. Jong, and W.K. Chandler. 1995. Calcium release and its voltage dependence in frog cut muscle fibers equilibrated with 20 mM EGTA. *J. Gen. Physiol.* 106:259–336. https://doi.org/10.1085/jgp.106.2.259

Pape, P.C., D.S. Jong, and W.K. Chandler. 1998. Effects of partial sarcoplasmic reticulum calcium depletion on calcium release in frog cut muscle fibers equilibrated with 20 mM EGTA. *J. Gen. Physiol.* 112:263–295. https://doi.org/10.1085/jgp.112.3.263

Pape, P.C., K. Fénelon, and N. Carrier. 2002. Extra activation component of calcium release in frog muscle fibres. *J. Physiol.* 542:867–886. https://doi.org/10.1113/jphysiol.2002.017095

Picollo, A., and M. Pusch. 2005. Chloride/proton antiporter activity of mammalian CLC proteins ClC-4 and ClC-5. *Nature.* 436:420–423. https://doi.org/10.1038/nature03720

Pitt, S.J., K.H. Park, M. Nishi, T. Urashima, S. Aoki, D. Yamazaki, J. Ma, H. Takeshima, and R. Sitsapesan. 2010. Charade of the SR K+-channel: Two ion-channels, TRIC-A and TRIC-B, masquerade as a single K+-channel. *Biophys. J.* 99:417–426. https://doi.org/10.1016/j.bpj.2010.04.051

Pizarro, G., and E. Ríos. 2004. How source content determines intracellular Ca^{2+} release kinetics. Simultaneous measurement of [Ca^{2+}] transients and [H$^+$] displacement in skeletal muscle. *J. Gen. Physiol.* 124:239–258. https://doi.org/10.1085/jgp.200409071

Rossi, D., C. Bencini, M. Maritati, F. Benini, S. Lorenzini, E. Pierantozzi, A.M. Scarcella, C. Paolini, F. Protasi, and V. Sorrentino. 2014. Distinct regions of triadin are required for targeting and retention at the junctional domain of the sarcoplasmic reticulum. *Biochem. J.* 458:407–417. https://doi.org/10.1042/BJ20130719

Rousseau, E., M. Roberson, and G. Meissner. 1988. Properties of single chloride selective channel from sarcoplasmic reticulum. *Eur. Biophys. J.* 16:143–151. https://doi.org/10.1007/BF00261900

Samsó, M. 2015. 3D structure of the dihydropyridine receptor of skeletal muscle. *Eur. J. Transl. Myol.* 25:4840. https://doi.org/10.4081/ejtm.2015.4840

Schneider, M.F. 1994. Control of calcium release in functioning skeletal muscle fibers. *Annu. Rev. Physiol.* 56:463–484. https://doi.org/10.1146/annurev.ph.56.030194.002335

Shaner, N.C., M.Z. Lin, M.R. McKeown, P.A. Steinbach, K.L. Hazelwood, M.W. Davidson, and R.Y. Tsien. 2008. Improving the photostability of bright monomeric orange and red fluorescent proteins. *Nat. Methods.* 5:545–551. https://doi.org/10.1038/nmeth.1209

Sharma, P., V. Ignatchenko, K. Grace, C. Ursprung, T. Kislinger, and A.O. Gramolini. 2010. Endoplasmic reticulum protein targeting of phospholamban: A common role for an N-terminal di-arginine motif in ER retention? *PLoS One.* 5:e11496. https://doi.org/10.1371/journal.pone.0011496

Smith, J.S., T. Imagawa, J. Ma, M. Fill, K.P. Campbell, and R. Coronado. 1988. Purified ryanodine receptor from rabbit skeletal muscle is the calcium-release channel of sarcoplasmic reticulum. *J. Gen. Physiol.* 92:1–26. https://doi.org/10.1085/jgp.92.1.1

Somlyo, A.V., H. Shuman, and A.P. Somlyo. 1977. Composition of sarcoplasmic reticulum in situ by electron probe X-ray microanalysis. *Nature.* 268:556–558. https://doi.org/10.1038/268556a0

Somlyo, A.V., H.G. Gonzalez-Serratos, H. Shuman, G. McClellan, and A.P. Somlyo. 1981. Calcium release and ionic changes in the sarcoplasmic reticulum of tetanized muscle: An electron-probe study. *J. Cell Biol.* 90:577–594. https://doi.org/10.1083/jcb.90.3.577

Somlyo, A.V., G. McClellan, H. Gonzalez-Serratos, and A.P. Somlyo. 1985. Electron probe X-ray microanalysis of post-tetanic Ca^{2+} and Mg^{2+} movements across the sarcoplasmic reticulum in situ. *J. Biol. Chem.* 260:6801–6807.

Sorrentino, V. 2011. Sarcoplasmic reticulum: Structural determinants and protein dynamics. *Int. J. Biochem. Cell Biol.* 43:1075–1078. https://doi.org/10.1016/j.biocel.2011.04.004

Sztretye, M., J. Yi, L. Figueroa, J. Zhou, L. Royer, P. Allen, G. Brum, and E. Ríos. 2011. Measurement of RyR permeability reveals a role of calsequestrin in termination of SR Ca^{2+} release in skeletal muscle. *J. Gen. Physiol.* 138:231–247. https://doi.org/10.1085/jgp.201010592

Tsien, R.Y. 1980. New calcium indicators and buffers with high selectivity against magnesium and protons: Design, synthesis, and properties of prototype structures. *Biochemistry.* 19:2396–2404. https://doi.org/10.1021/bi00552a018

Tsutsui, H., S. Karasawa, Y. Okamura, and A. Miyawaki. 2008. Improving membrane voltage measurements using FRET with new fluorescent proteins. *Nat. Methods.* 5:683–685. https://doi.org/10.1038/nmeth.1235

Tsutsui, H., Y. Jinno, A. Tomita, Y. Niino, Y. Yamada, K. Mikoshiba, A. Miyawaki, and Y. Okamura. 2013a. Improved detection of electrical activity with a voltage probe based on a voltage-sensing phosphatase. *J. Physiol.* 591:4427–4437. https://doi.org/10.1113/jphysiol.2013.257048

Tsutsui, H., Y. Jinno, A. Tomita, and Y. Okamura. 2013b. Optically detected structural change in the N-terminal region of the voltage-sensor domain. *Biophys. J.* 105:108–115. https://doi.org/10.1016/j.bpj.2013.05.051

Vergara, J., F. Bezanilla, and B.M. Salzberg. 1978. Nile blue fluorescence signals from cut single muscle fibers under voltage or current clamp conditions. *J. Gen. Physiol.* 72:775–800. https://doi.org/10.1085/jgp.72.6.775

Wang, J., and P.M. Best. 1994. Characterization of the potassium channel from frog skeletal muscle sarcoplasmic reticulum membrane. *J. Physiol.* 477:279–290. https://doi.org/10.1113/jphysiol.1994.sp020190

Yazawa, M., C. Ferrante, J. Feng, K. Mio, T. Ogura, M. Zhang, P.H. Lin, Z. Pan, S. Komazaki, K. Kato, et al. 2007. TRIC channels are essential for Ca^{2+} handling in intracellular stores. *Nature.* 448:78–82. https://doi.org/10.1038/nature05928